PAPER

Phase-field modeling for 3D grain growth based on a grain boundary energy database

To cite this article: Hyun-Kyu Kim *et al* 2014 *Modelling Simul. Mater. Sci. Eng.* **22** 034004

View the article online for updates and enhancements.

Related content

- Influence of anisotropic grain boundary properties on the evolution of grain boundary character distribution during grain growth—a 2D level set study
  Håkan Hallberg

- A two-dimensional study of coupled grain boundary motion using the level set method
  Anup Basak and Anurag Gupta

- Phase field modeling of the effect of porosity on grain growth kinetics in polycrystalline ceramics
  K Ahmed, C A Yablinsky, A Schulte et al.

Recent citations

- Phase-field modeling of crystal nucleation in undercooled liquids – A review
  László *et al*

- Phase field modeling of stressed grain growth: effect of inclination and misorientation dependence of grain boundary energy
  E. Shahnooshi *et al*

- A three-dimensional misorientation axis- and inclination-dependent Kobayashi–Warren–Carter grain boundary model
  Nikhil Chandra Admal *et al*

Phase-field modeling for 3D grain growth based on a grain boundary energy database

Hyun-Kyu Kim[1]**, Seong Gyoon Kim**[2]**, Weiping Dong**[1]**, Ingo Steinbach**[3] **and Byeong-Joo Lee**[1,4]

[1] Department of Materials Science and Engineering, Pohang University of Science and Technology (POSTECH), Pohang 790-784, Korea
[2] Department of Materials Science and Engineering, Kunsan National University, Kunsan 573-701, Korea
[3] Interdisciplinary Centre for Advanced Materials Simulation (ICAMS), Ruhr-University Bochum, 44801 Bochum, Germany

E-mail: calphad@postech.ac.kr

Abstract

A 3D phase-field model for grain growth combined with a grain boundary (GB) energy database is proposed. The phase-field model is applied to a grain growth simulation of polycrystalline bcc Fe to investigate the effect of anisotropic GB energy on the microstructural evolution and its kinetics. It is found that the anisotropy in the GB energy results in different microstructures and slower kinetics, especially when the portion of low-angle, low-energy GBs is large. We discuss the applicability of the proposed phase-field simulation technique, based on the GB or interfacial energy database to simulations for microstructural evolution, including abnormal grain growth, phase transformations, etc., in a wider range of polycrystalline materials.

Keywords: phase-field model, grain growth, anisotropic grain boundary energy, grain boundary energy database

(Some figures may appear in colour only in the online journal)

S Online supplementary data available from stacks.iop.org/MSMSE/22/034004/mmedia

[4] Author to whom any correspondence should be addressed.

1. Introduction

Microstructure evolution is important because it has a strong influence on the mechanical, thermal and electrical properties of engineering materials [1, 2]. Grain growth is a typical microstructure evolution involved in various phenomena such as the disappearance of grains, merging of boundaries, face switching and other topological singularities [3], which reduce the total amount of grain boundary (GB) energy. This topic has been extensively studied using experiments, modeling and simulation methods [4, 5].

The phase-field model is a typical method to investigate microstructural phenomena with complex morphology such as phase transformations, recrystallizations, etc. [1–3, 6–11]. With its ability to describe the curvature effect naturally and accurately, it has proven to be suitable for the study of grain growth-related phenomena [10–29]. Chen and Yang proposed a multi-order model [12] assigning N order parameters to N allowed orientations. This model has been modified and extended by Fan and Chen [13] and by Krill and Chen [14] for two-dimensional (2D) and three-dimensional (3D) simulations of grain coarsening. Steinbach *et al* [15] proposed a phase-field concept for multiphase systems, which has the constraint that the sum of all order parameters should be one. This model has been used to investigate statistical and topological perspectives of ideal grain growth [16] and to study grain growth behavior in thin films [17]. Kazaryan *et al* [18–20] and Suwa *et al* [21, 22] studied 2D grain growth kinetics and morphological evolution on the basis of schematically introduced anisotropy in GB energy and mobility. Kobayashi *et al* [23] suggested a 2D phase-field model for GB motion using only two variables: an indicator of the mean orientation of crystals and an order parameter for the degree of crystal orientation. This model could be distinct from others mentioned above in that it does not have an order parameter per orientation. It has some advantages because of this and has now been extended to 3D using quaternions [24, 25]. The phase-field model introduced by Kim *et al* has certain advantages in modeling grain growth with anisotropic GB properties (GB energy and mobility) [26] and in dealing with thousands of grains efficiently [1]. Moelans *et al* [27, 28] and McKenna *et al* [3] introduced a phase-field formulation for grain growth that can account for arbitrary disorientation angles and axis dependence of GB properties. Upmanyu *et al* [29] studied the effects of anisotropy in GB energy and mobility using a 2D phase-field simulation.

Most of these studies have indicated that GB properties play a decisive role in grain growth kinetics and morphological evolution. In the industrial field of electrical steel products, which utilises abnormal grain growth phenomena, many experimental studies have been carried out to clarify the relationship between the growth of Goss-oriented grains and the anisotropy of GB properties during secondary recrystallization [30, 31]. Therefore, it is highly recommended to consider the realistic anisotropy of GB properties in grain growth modeling and simulations. Even with its importance for the realistic anisotropy of GB properties, no phase-field simulation combined with realistic GB properties has been performed. This is because sufficient information for the anisotropy in properties of all possible GBs has not been available. Recently, Kim *et al* [32] proposed a scheme to identify individual GBs on the basis of five macroscopic degrees of freedom (three from the misorientation and two from the inclination) and calculated energies of systematically selected grain GBs in pure Fe using an atomistic approach (molecular statics). The calculated GB energy values were provided in the form of a GB energy database so that a phase-field model based on realistic GB energy could be developed and an investigation into the effect of anisotropic GB energy on microstructural evolution and its kinetics would become feasible in a future study.

Such an attempt is now made in the present work. The purpose of the present work is to provide a new phase-field model combined with a realistic GB energy database, by extending
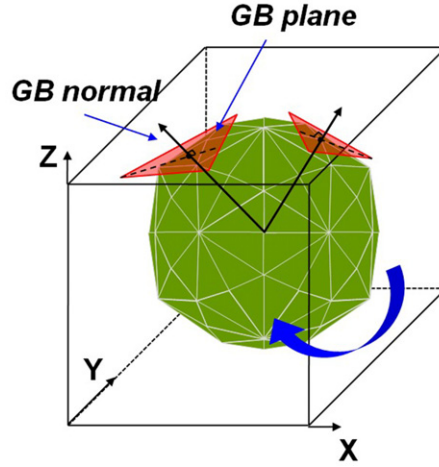
Figure 1. A scheme to identify individual GBs with discrete inclination angles between two neighboring grains under a given misorientation [32].

the previously developed phase-field model for grain growth simulation [1] so that it can utilise the recently developed GB energy database [32]. The phase-field model is applied to simulate grain growth in polycrystalline bcc Fe and to investigate the effect of anisotropy in GB energy on the microstructural evolution and grain growth kinetics. Following this introductory section, we briefly describe how to construct the GB energy database. In section 3, the new phase-field model and various assumptions made for the implementation of the GB energy database are presented. In section 4, grain growth simulation results based on the anisotropic GB energy are discussed and compared with those based on isotropic GB energy. The main points obtained in the present study are summarised in section 5.

2. Construction of the GB energy database

A GB between two grains is uniquely defined in a 3D space when five macroscopic degrees of freedom (misorientation and inclination angles) are fixed. There are several ways to identify individual GBs based on the five degrees of freedom [32, 33]. The main difference comes from whether the misorientation and inclination are considered separately [32] or simultaneously [33] in the five-dimensional space. In the present work, we use the scheme recently proposed with the GB energy database [32]. To identify individual GBs between two neighbouring grains, consider a polyhedron inside a cube with the three [1 0 0] axes parallel to the x, y and z directions. Then, imagine that the two neighbouring grains in a polycrystalline sample are rotated such that the crystallographic orientation of one grain corresponds to the cube orientation and the orientation of the other grain to that of the polyhedron inside the cube, as shown in figure 1. It should be noted in figure 1 that the polyhedron involves many surfaces. The misorientation between the cube and the polyhedron, which can be uniquely defined by three Euler angles, corresponds to the misorientation between the two grains. The surfaces of the polyhedron correspond to GBs between the two grains at different inclination angles, and can be uniquely defined by two degrees of freedom (polar and azimuthal angles) [32].

To practically construct a GB energy database, the misorientation and inclination angles must be discretised. In the present work, the misorientation angle is divided into nine equal intervals (10°) in the range $0° \leqslant \phi_1, \Phi, \phi_2 \leqslant 90°$, and the inclination angles

are selected at directions perpendicular to the 60 surface planes and 31 vertices of the polyhedron, avoiding duplications from crystal symmetry. The GB database obtained by mechanically dividing the misorientation angle cannot sufficiently include the special boundaries formed at specific misorientations, which are usually believed to play an important role in morphological evolution, with relatively low energies compared to other high-angle boundaries. To supplement this problem, special boundaries (26 coincidence site lattice boundaries corresponding to $\Sigma \leqslant 33$) are selected and their database is constructed separately. In addition, low-angle GBs (LAGBs) with six misorientations (Euler angles)—($(0\,0\,5)$, $(0\,5\,0)$, $(5\,0\,0)$, $(0\,5\,5)$, $(5\,5\,0)$ and $(5\,5\,5)$)—are also added to the database because the present discretization by $10°$ is thought to be insufficient for LAGBs. Therefore, the number of GBs in the present database totals 69 251, comprising 66 339 from mechanically selected GBs based on the discrete misorientation and inclination angles, and 2912 (32×91) from intentionally selected special boundaries (26 sets) and LAGBs (6 sets).

3. Implementation of the discrete GB energy database into the phase-field model

To implement the GB energy database into the phase-field simulation, basic governing equations related to the GB energy and its second derivative with respect to inclination angles need to be modified. Before that, procedures to identify the misorientation between neighboring grains and to identify the inclination of GB under the given misorientation need to be developed. The details of those procedures and the relevant governing equation are described in this section.

3.1. Determination of misorientation between two neighboring grains

The misorientation between two neighboring grains should first be identified in order to obtain the GB energy information from the GB energy database. The misorientation between neighboring grains can be easily obtained by a tensor operation, $\Delta g = g_a g_b^{-1}$, between the rotation tensors (g_a and g_b) for the two grains, which are defined from the three Euler angles describing the orientation of each grain. Due to the crystallographic symmetry of the cubic structure, there may be many equivalent misorientation relationships. However, the present GB energy database considers only the misorientation that can be represented by three Euler angles satisfying $0° \leqslant \phi_1, \Phi, \phi_2 \leqslant 90°$. Therefore, the misorientation tensor is pre- and post-multiplied by cubic symmetry operators so that the above criterion for the Euler angles is satisfied. Then, the resultant misorientation is compared with those registered in the GB energy database using the quaternion method [34], and the registered misorientation closest to that between the two grains is finally selected.

If a polycrystalline system consisting of Q grains is given, the number of available misorientations is equal to $_QC_2$. In the present work, to save simulation time, all available misorientations among grains in the system are calculated in advance, and a misorientation table is created as shown in figure 2. Therefore, if a GB is newly created during a grain growth simulation, information corresponding to its misorientation can easily be found from the misorientation table.

3.2. Estimation of GB energy for a given inclination

Section 3.1 describes how the misorientation between two neighboring grains is identified in the present work. Once the misorientation is determined, it is necessary to identify the
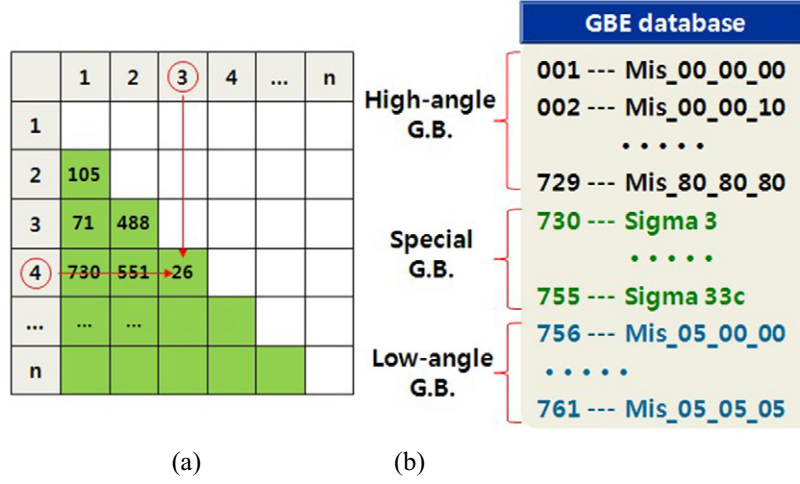
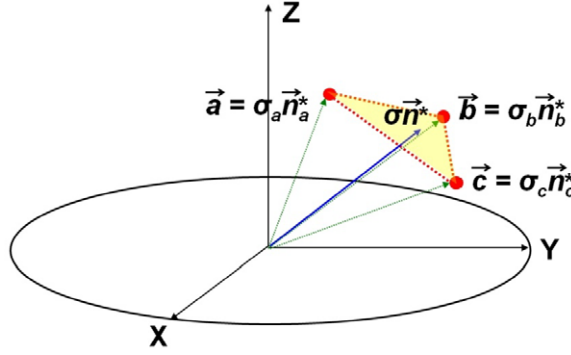**Figure 2.** (*a*) A pre-constructed misorientation table and (*b*) the structure of the GB energy database.

Figure 3. The relation between the energy (σ) of a GB with a specific inclination angle ($\vec{n}^*$) and the energy ($\sigma_a, \sigma_b, \sigma_c$) of GBs with surrounding, registered inclination angles ($\vec{n}_a^*, \vec{n}_b^*, \vec{n}_c^*$) on the surface of a γ-plot.

inclination and obtain the corresponding GB energy value, which will be described in the present section.

The GB energy database constructed by Kim *et al* [32] includes 91 data points with different inclination angles for each misorientation. The directions from the center of the polyhedron to the surface planes or surface corners (vertices) of the polyhedron correspond to the GB normal directions based on the crystallographic coordinates of one grain (those in figure 1), as mentioned previously, and are registered in the database. However, the inclination of an arbitrary GB between two grains would not match exactly with one of the registered inclination angles in the database, but would exist mostly between several. Now, imagine a 3D γ-plot instead of the polyhedron, with the origin of the plot at the center of the polyhedron. Figure 3 shows part of surface of the γ-plot for the inclination of an arbitrary GB (designated by a vector $\vec{n}^*$). In the present article, '*' represents quantities based on crystallographic coordinates, not sample coordinates. Figure 3 shows the probable relation between the inclination ($\vec{n}^*$) of the

arbitrary GB under consideration and those of surrounding GBs ($\vec{n}_a^*$, $\vec{n}_b^*$ and $\vec{n}_c^*$) registered in the database. The distances from the origin to the individual points represent registered GB energy (σ_a, σ_b and σ_c) on the corresponding inclination angle. A GB energy value should be assigned to the GB under consideration (with the inclination $\vec{n}^*$). In the present study, it is assumed that the GB energy for the GB under consideration corresponds to the weighted average of the three nearest data points ($\vec{a}^*$, $\vec{b}^*$ and $\vec{c}^*$) shown in figure 3. Therefore, assigning the GB energy is now reduced to a mathematical problem to find the σ value, the radial distance to the point where $\vec{n}^*$ intersects the triangular plane defined by the three points $\vec{a}^*$, $\vec{b}^*$ and $\vec{c}^*$. The GB energy σ can be represented by

$$\sigma = \frac{a_1^* A^* + a_2^* B^* + a_3^* C^*}{n_1^* A^* + n_2^* B^* + n_3^* C^*}, \tag{1}$$

where n_i^*, a_i^*, b_i^* and c_i^* ($i = 1, 2, 3$) correspond to components of vectors $\vec{n}^*$, $\vec{a}^*$, $\vec{b}^*$ and $\vec{c}^*$, respectively, and A^*, B^* and C^* are constants that can be expressed using the components of the following vectors:

$$A^* = (a_2^* - b_2^*)(a_3^* - c_3^*) - (a_2^* - c_2^*)(a_3^* - b_3^*), \tag{2}$$

$$B^* = (a_1^* - c_1^*)(a_3^* - b_3^*) - (a_1^* - b_1^*)(a_3^* - c_3^*)$$

$$C^* = (a_1^* - b_1^*)(a_2^* - c_2^*) - (a_1^* - c_1^*)(a_2^* - b_2^*).$$

The mathematical approach described above is valid only when the three neighboring data points can be selected so that the normal vector $\vec{n}^*$ representing the inclination of the GB under consideration intersects the triangular plane defined by the three data points. However, it should be noted here that the 91 discrete inclination angles are not uniformly distributed in the 3D space (see figure 1). Such non-uniformity can cause situations where several different triangular planes are defined for one normal vector $\vec{n}^*$ and even the normal vector $\vec{n}^*$ does not intersect the triangular plane defined by the three data points selected. This problem could be solved by pre-assigning data point sets to define suitable triangular planes.

It has been shown that the GB energy at an arbitrary inclination between two neighboring grains can be uniquely and continuously obtained by finding three data points with neighboring inclination angles in the GB energy database (as shown in figure 3) and taking the weighted average of the energy values on the three neighboring data points. For a special boundary with a specific misorientation and inclination, the exact misorientation can be found in the present GB energy database because a special database is operated for those special boundaries as mentioned in section 2. However, it should be clearly mentioned here that the exact inclination for a special boundary with a given misorientation would be mostly missed in the database. This is because the inclination angles dealt with in the present database are those mechanically discretised using the polyhedron shown in figure 1, without considering the exact inclination angles for special boundaries. Therefore, instead of cusp point values, only an approximate value, i.e. the average of the values at neighboring inclination angles would be obtained for the GB energy and its derivatives with respect to the inclination angles according to the present GB energy database, which should be further improved in future work.

It should also be emphasised here that the simulation is performed based on 'specimen coordinates' (computational coordinates), while the GB energy database is constructed based on 'crystallographic coordinates', where the orientation of one grain that forms the GB corresponds to the cube orientation, as illustrated in figure 1. To obtain the GB energy of a specific GB under consideration during the phase-field simulation, first, the GB normal is determined. The components of the GB normal vector ($\vec{n}$) are based on the specimen coordinates at this stage. The GB normal vector is rotated using a rotation tensor so that the

orientation of one grain corresponds to the cube orientation; that is, the vector components are those based on the crystallographic coordinates. This rotated normal vector ($\vec{n}^*$) is used to find the normal vectors ($\vec{n}_a^*$, $\vec{n}_b^*$, $\vec{n}_c^*$) for neighboring data points and GB energy (σ_a, σ_b, σ_c) at each point in the database (see figure 3). Those quantities can be used for computing the inclination dependence of the GB energy as well as the GB energy value itself for the GB under consideration. However, before computing the inclination dependence, the normal vectors ($\vec{n}_a^*$, $\vec{n}_b^*$, $\vec{n}_c^*$) for neighboring points and the normal vector ($\vec{n}^*$) for the GB under consideration are rotated back to the specimen coordinates using the inverse of the same rotation tensor that was used to rotate the normal vector ($\vec{n}$) from the specimen coordinates to the crystallographic coordinates. After this operation, the components of the vectors ($\vec{a}^*$, $\vec{b}^*$ and $\vec{c}^*$) in figure 3 become those based on the specimen coordinates, and are used to find the inclination dependence of the GB energy through the procedure, as described in the next section.

3.3. Phase-field modeling for implementation of the GB energy database

A phase-field grain growth simulation based on the anisotropic GB energy database indicates that the simulation is performed over a polycrystalline system where each grain is assigned its own crystallographic orientation. When the polycrystalline system consists of Q grains in a phase-field simulation, the orientation state of a grid point is defined by phase-field variables ϕ_i ($i = 1, 2, \ldots, Q$). Here, the integer i indicates the orientation of the ith grain, and we impose a condition that the sum of all phase fields at any position in the system is conserved [1],

$$Z \equiv \sum_{i=1}^{Q} \phi_i = 1. \tag{3}$$

In the present work, the time evolution equation of ϕ_i is formulated by the interface field method proposed by Steinbach and Pezzolla [2]. According to Kim *et al* [1], the advantage of this method for grain growth modeling is that the force balances are exactly maintained at triple points and the anisotropic GB properties can be easily implemented.

The total free energy functional of a single element system of volume V is given by

$$F = \int [f_{GB} + \lambda(Z - 1)]\,\mathrm{d}V, \tag{4}$$

where λ is the Lagrange multiplier that accounts for the constraint equation (3) and is cancelled out later on. f_{GB} is the excess free energy due to the existence of the GB, defined by

$$f_{GB} = \sum_{i=1}^{Q} \sum_{j>i}^{Q} \left(-\frac{\varepsilon_{ij}^2}{2} \nabla\phi_i \cdot \nabla\phi_j + \omega_{ij}\phi_i\phi_j \right), \tag{5}$$

where ε_{ij} is the gradient energy coefficient and ω_{ij} is the height of the double obstacle potential. Since the phase field ϕ can take on values less than zero or greater than one, a cut-off is introduced as described in [1], which is omitted here for readability. We define a step function: $s_i = 1$ if $\phi_i > 0$ and $s_i = 0$ otherwise. Then, the number of grains coexisting in a given point is

$$S(x) = \sum_{i=1}^{Q} s_i(x). \tag{6}$$

The evolution equation of the phase field can be derived as

$$\frac{\partial \phi_i}{\partial t} = -\frac{2M_\phi}{S} \sum_{\substack{j \neq i}}^{Q} s_i s_j \left[\frac{\delta F}{\delta \phi_i} - \frac{\delta F}{\delta \phi_j} \right], \tag{7}$$

where M_ϕ is the phase-field mobility. If the GB energy is isotropic or is dependent only on the misorientation angle, the functional derivatives in equation (7) are given by

$$\frac{\delta F}{\delta \phi_i} = \sum_{j \neq i}^{Q} \left[\frac{\varepsilon_{ij}^2}{2} \nabla^2 \phi_j + \omega_{ij} \phi_j \right]. \tag{8}$$

Equations (7) and (8) are the phase-field equations for GB movement between grain i and grain j. The three parameters, ε, ω and M_φ in equations (7) and (8) are related to the energy σ, width 2ξ and mobility m of the GB [1, 2, 35] as follows:

$$\omega_{ij} = \frac{2\sigma_{ij}}{\xi_{ij}}, \qquad \varepsilon_{ij} = \frac{4}{\pi} \sqrt{\xi_{ij} \sigma_{ij}}, \qquad M_{\phi,ij} = \frac{\pi^2}{16\xi_{ij}} m_{ij}. \tag{9}$$

All parameter values can be determined once the relevant material property values (energy, GB width and mobility) are given. Then, the grain growth behavior can be simulated by numerically solving equations (7) and (8). However, it should be mentioned that equations (7) and (8) are valid only when the gradient energy coefficient ε_{ij} can be regarded as constant and independent from the inclination which is a function of the phase-field variable, ϕ_i. If this parameter is dependent on the inclination and thus on the phase-field variable, the functional derivatives, equation (8), should be derived again from equations (4) and (5), as has been done by Karma and Rappel [7] and by Kim [36].

The phase-field model proposed in the present study can consider the inclination dependency of GB energy σ given by equation (1). The normal vector $\vec{n}_{ij}$ perpendicular to the GB between grains i and j can be denoted as

$$\vec{n}_{ij} = \frac{\nabla \psi_{ij}}{\left| \nabla \psi_{ij} \right|}. \tag{10}$$

Here, we introduce the difference of a pair phase-field $\psi_{ij} \equiv \phi_i - \phi_j$. This function must not be confused with the interface fields as introduced in [2] for multiple junctions, since higher order contributions are neglected here. The term that gives rise to the inclination dependence of the GB energy in equations (4) and (5) is now rewritten as follows:

$$F_{ij} = \int \frac{\varepsilon_{ij}(\vec{n}_{ij})^2}{2} \nabla \phi_i \cdot \nabla \phi_j \, \mathrm{d}V. \tag{11}$$

By applying the following variational derivative to equation (11),

$$\frac{\delta}{\delta \phi_i} = \frac{\partial}{\partial \phi_i} - \nabla \cdot \frac{\partial}{\partial (\nabla \phi_i)} = \frac{\partial}{\partial \phi_i} - \frac{\partial}{\partial x} \left(\frac{\partial}{\partial (\partial_x \phi_i)} \right) - \frac{\partial}{\partial y} \left(\frac{\partial}{\partial (\partial_y \phi_i)} \right) - \frac{\partial}{\partial z} \left(\frac{\partial}{\partial (\partial_z \phi_i)} \right), \tag{12}$$

one can obtain the new expression for the functional derivatives as

$$\frac{\delta F_{ij}}{\delta \phi_i} = -\nabla \cdot \frac{\partial}{\partial (\nabla \phi_i)} \left(\frac{\varepsilon_{ij}(\vec{n}_{ij})^2}{2} \nabla \phi_i \cdot \nabla \phi_j \right)$$

$$= -\nabla \cdot \frac{\varepsilon_{ij}(\vec{n}_{ij})^2}{2} \frac{\partial}{\partial (\nabla \phi_i)} (\nabla \phi_i \cdot \nabla \phi_j) - \nabla \cdot (\nabla \phi_i \cdot \nabla \phi_j) \frac{\partial}{\partial (\nabla \phi_i)} \left(\frac{\varepsilon_{ij}(\vec{n}_{ij})^2}{2} \right)$$

$$= -\nabla \cdot \left(\frac{\varepsilon_{ij}(\vec{n}_{ij})^2}{2} \cdot \nabla \phi_j \right) - \frac{\partial}{\partial x} \left(\nabla \phi_i \cdot \nabla \phi_j \varepsilon_{ij}(\vec{n}_{ij}) \frac{\partial \varepsilon_{ij}(\vec{n}_{ij})}{\partial (\partial_x \phi_i)} \right)$$

$$- \frac{\partial}{\partial y} \left(\nabla \phi_i \cdot \nabla \phi_j \varepsilon_{ij}(\vec{n}_{ij}) \frac{\partial \varepsilon_{ij}(\vec{n}_{ij})}{\partial (\partial_y \phi_i)} \right) - \frac{\partial}{\partial z} \left(\nabla \phi_i \cdot \nabla \phi_j \varepsilon_{ij}(\vec{n}_{ij}) \frac{\partial \varepsilon_{ij}(\vec{n}_{ij})}{\partial (\partial_z \phi_i)} \right). \tag{13}$$

Equations (7) and (13) are the phase-field equations for the movement of a GB with inclination-dependent GB energy between grain i and grain j.

In order to obtain mathematical expressions for the three derivative terms on ε_{ij} in equation (13), a functional form of inclination should be given to the gradient energy coefficient ε_{ij}. Under the correlation between the GB energy and the gradient energy coefficient, the functional form of the gradient energy coefficient $\varepsilon_{ij}(\vec{n}_{ij})$ should be given the same form as the GB energy $\sigma_{ij}(\vec{n}_{ij})$. The functional form of the GB energy, equation (1), proposed in the present study can be rewritten for a GB between grain i and grain j as follows, based on the specimen coordinates:

$$\sigma_{ij}(\vec{n}_{ij}) = \frac{a_1 A + a_2 B + a_3 C}{n_{ij,1} A + n_{ij,2} B + n_{ij,3} C}. \tag{14}$$

Here, a_1, a_2, a_3, A, B and C are constants which are obtained from the three nearest data points in the GB energy database (see figure 3) through a rotation back to the specimen coordinates from the crystallographic coordinates, as described already.

Similarly, the gradient energy coefficient $\varepsilon_{ij}(\vec{n}_{ij})$ is expressed as follows:

$$\varepsilon_{ij}(\vec{n}_{ij}) = \frac{E \varepsilon_0}{n_{ij,1} A + n_{ij,2} B + n_{ij,3} C}, \tag{15}$$

where $E = (a_1 A + a_2 B + a_3 C)$, and ε_0 is a constant that connects the GB energy and gradient energy coefficient. Each component of $\vec{n}_{ij}$ is given by

$$\vec{n}_{ij,1} = \frac{\partial_x \psi_{ij}}{|\nabla \psi_{ij}|}; \qquad \vec{n}_{ij,2} = \frac{\partial_y \psi_{ij}}{|\nabla \psi_{ij}|}; \qquad \vec{n}_{ij,3} = \frac{\partial_z \psi_{ij}}{|\nabla \psi_{ij}|}. \tag{16}$$

Then, equation (15) can be modified into

$$\varepsilon_{ij}(\vec{n}_{ij}) = \varepsilon_0 \frac{E |\nabla \psi_{ij}|}{A \partial_x \psi_{ij} + B \partial_y \psi_{ij} + C \partial_z \psi_{ij}}. \tag{17}$$

In this study, the inclination of a point in the interfacial region is defined by the gradient of ψ_{ij} as in equation (10). Therefore the inclination dependence in the final three terms of equation (13) should be transformed into the dependence on the gradient of ψ_{ij}. This transformation can be done straightforwardly, as follows

$$\frac{\partial \varepsilon_{ij}(\vec{n}_{ij})}{\partial(\partial_x \phi_i)} = \frac{\partial \varepsilon_{ij}(\vec{n}_{ij})}{\partial(\partial_x \psi_{ij})} = E \varepsilon_0 \frac{\partial}{\partial(\partial_x \psi_{ij})} \left(\frac{|\nabla \psi_{ij}|}{A \partial_x \psi_{ij} + B \partial_y \psi_{ij} + C \partial_z \psi_{ij}} \right)$$
$$= E \varepsilon_0 \left(\frac{\partial_x \psi_{ij}/|\nabla \psi_{ij}|}{A \partial_x \psi_{ij} + B \partial_y \psi_{ij} + C \partial_z \psi_{ij}} - \frac{A |\nabla \psi_{ij}|}{(A \partial_x \psi_{ij} + B \partial_y \psi_{ij} + C \partial_z \psi_{ij})^2} \right). \tag{18}$$

This equation can be rewritten as

$$\frac{\partial \varepsilon_{ij}(\vec{n}_{ij})}{\partial(\partial_x \phi_i)} = E \varepsilon_0 \frac{(\partial_x \psi_{ij})(A \partial_x \psi_{ij} + B \partial_y \psi_{ij} + C \partial_z \psi_{ij}) - A |\nabla \psi_{ij}|^2}{|\nabla \psi_{ij}|(A \partial_x \psi_{ij} + B \partial_y \psi_{ij} + C \partial_z \psi_{ij})^2}, \tag{19}$$

one of the differential terms in equation (13). Using the same approach, the other two terms are written as

$$\frac{\partial \varepsilon_{ij}(\vec{n}_{ij})}{\partial(\partial_y \phi_i)} = E \varepsilon_0 \frac{(\partial_y \psi_{ij})(A \partial_x \psi_{ij} + B \partial_y \psi_{ij} + C \partial_z \psi_{ij}) - B |\nabla \psi_{ij}|^2}{|\nabla \psi_{ij}|(A \partial_x \psi_{ij} + B \partial_y \psi_{ij} + C \partial_z \psi_{ij})^2} \tag{20}$$

$$\frac{\partial \varepsilon_{ij}(\vec{n}_{ij})}{\partial(\partial_z \phi_i)} = E \varepsilon_0 \frac{(\partial_z \psi_{ij})(A \partial_x \psi_{ij} + B \partial_y \psi_{ij} + C \partial_z \psi_{ij}) - C |\nabla \psi_{ij}|^2}{|\nabla \psi_{ij}|(A \partial_x \psi_{ij} + B \partial_y \psi_{ij} + C \partial_z \psi_{ij})^2}.$$

Multiplying these equations by ε_{ij} yields

$$\varepsilon_{ij} \frac{\partial \varepsilon_{ij}}{\partial(\partial_x \phi_i)} = E^2 \varepsilon_0^2 \frac{(\partial_x \psi_{ij})(A \partial_x \psi_{ij} + B \partial_y \psi_{ij} + C \partial_z \psi_{ij}) - A |\nabla \psi_{ij}|^2}{(A \partial_x \psi_{ij} + B \partial_y \psi_{ij} + C \partial_z \psi_{ij})^3} \tag{21}$$
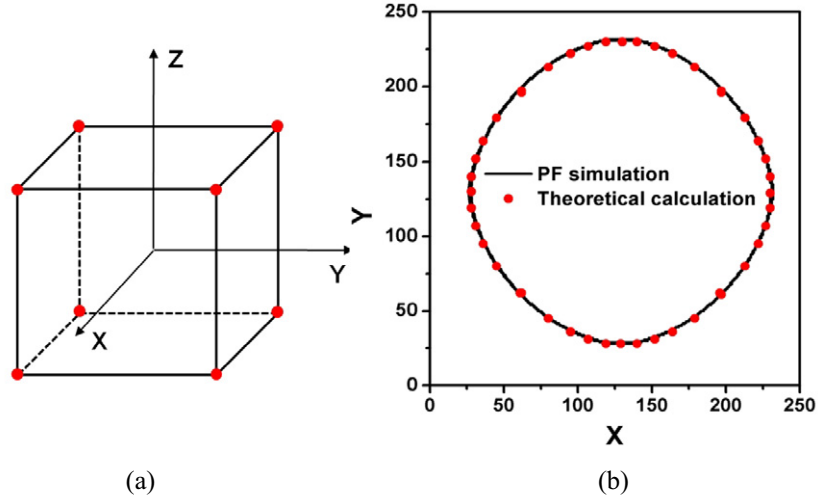
Figure 4. (*a*) A γ-plot for an artificially assigned cubic anisotropy in GB energy between an island grain and a surrounding grain, and (*b*) the resultant equilibrium shape of the island grain on the (1 0 0) plane.

$$\varepsilon_{ij}\frac{\partial \varepsilon_{ij}}{\partial\left(\partial_y \phi_i\right)} = E^2\varepsilon_0^2 \frac{\left(\partial_y \psi_{ij}\right)\left(A\partial_x\psi_{ij} + B\partial_y\psi_{ij} + C\partial_z\psi_{ij}\right) - B\left|\nabla\psi_{ij}\right|^2}{\left(A\partial_x\psi_{ij} + B\partial_y\psi_{ij} + C\partial_z\psi_{ij}\right)^3}$$

$$\varepsilon_{ij}\frac{\partial \varepsilon_{ij}}{\partial\left(\partial_z \phi_i\right)} = E^2\varepsilon_0^2 \frac{\left(\partial_z \psi_{ij}\right)\left(A\partial_x\psi_{ij} + B\partial_y\psi_{ij} + C\partial_z\psi_{ij}\right) - C\left|\nabla\psi_{ij}\right|^2}{\left(A\partial_x\psi_{ij} + B\partial_y\psi_{ij} + C\partial_z\psi_{ij}\right)^3}.$$

Equation (21) is inserted into equation (13) and applied to equation (7) to obtain the final phase-field equation.

4. Effect of anisotropic GB energy on grain growth

The phase-field model combined with the discrete GB energy database is now available and ready for a simulation of grain growth to investigate the effect of anisotropic GB energy on microstructural evolution and its kinetics. Before performing grain growth simulations, it is necessary to confirm that the GB energy database is correctly implemented in the phase-field simulation code. For this, a simple test simulation [7] is performed for the morphological evolution of an isolated crystal of a fixed volume inside a surrounding grain, on the basis of an artificially designed cubic anisotropy of the GB energy. It should be remembered that if the GB energy is anisotropic, the equilibrium shape of a grain follows a Wulff construction. Figure 4(*a*) is the gamma plot used in the test simulation, which shows that the GB energy is the minimum along ⟨1 0 0⟩ directions, while it is the maximum for ⟨1 1 1⟩ directions. In this case, the island grain changes its shape into a convex regular octahedron during the simulation. The equilibrium shape can also be obtained theoretically from the sharp-interface theory [37, 38]. The simulated and theoretical equilibrium shapes on a {1 0 0} plane are compared in figure 4(*b*). The agreement is very good, which indicates that the present phase-field code correctly implements the GB energy database.

In multi-grain growth simulations, the number of phase-field variables required for each grid point is the same as the total number of grains included in simulation samples. An

extremely large memory space is required to deal with such a large number of phase-field variables. To overcome this problem, the maximum number of phase fields coexisting on each grid point is restricted to seven in the present study, based on the previously developed scheme [1, 39, 40]. The size of the polycrystalline sample prepared in the present study is $200 \times 200 \times 200$ grid points with about 1300 grains. The initial grain size distribution in the polycrystalline sample is obtained by putting spherical grains on randomly sampled positions. The crystallographic orientations of the individual grains are assigned randomly or introducing a texture component, as will be mentioned in more detail later on. The radii of the grains are also randomly sampled within a predetermined range of 14–18 grid points. To minimise the boundary effect on the grain growth kinetics, periodic boundary conditions are given along all directions. The GB thickness is resolved by four grid points ($2\xi = 4\Delta x$), which appears to be a good compromise between high computational efficiency and negligible grid anisotropy. In addition to the grain growth simulation based on the anisotropic GB energy database of bcc Fe [32], one more series of simulations is performed, assigning an average constant value ($1.2\,\mathrm{J\,m^{-2}}$) to the energy of all GBs for comparison. The GB mobility is given a constant value of $1.0 \times 10^{-11}\,\mathrm{m^4\,J\,s^{-1}}$ which corresponds to a value of fcc/bcc interface mobility in Fe alloys at 1000 K according to Wits *et al* [41]. To simulate the grain growth in usual polycrystalline systems with micrometer-scale average grain size, a grid size of $\Delta x = \Delta y = \Delta z = 0.2\,\mu\mathrm{m}$ is adopted. The time step is given a value of $\Delta t = 3.33 \times 10^{-4}\,\mathrm{s}$, within half of the numerical stability limit.

In the present work, two different crystallographic orientations of the individual grains are considered, as mentioned above: one with randomly assigned crystallographic orientations for individual grains and the other with a weak texture. In the latter case, 5.1% of the GBs are LAGBs (misorientation <10°), while the portion of LAGBs is 1.4% in the case of the randomly orientated polycrystalline structure. Three simulations are performed varying the crystallographic orientation and anisotropy of the GB energy: one with random crystallographic orientation and isotropic GB energy, one with random crystallographic orientation and anisotropic GB energy, and one with weakly textured crystallographic orientation and anisotropic GB energy. Figure 5 shows the microstructural evolution in each of the three systems. No apparent difference is observed in the microstructure among the three systems up to 10 000 time steps (3.3 s) since the present simulation covers only an initial stage of grain growth in a relatively small sample. Various analyses (growth kinetics, grain size distribution, misorientation distribution, number of faces per grain, etc.) are carried out to examine the effect of anisotropic GB energy on the grain growth behavior in more detail.

Before further analyses, it is necessary to confirm that the simulation reproduces the well-known parabolic growth law for normal grain growth [14, 42]:

$$\langle r(t) \rangle^2 - \langle r(0) \rangle^2 = kt, \tag{22}$$

where $\langle r(t) \rangle$ is the average grain size at time t, and k is a rate constant. Figures 6(*a*) and (*b*) show the evolution of the average grain size and number of remaining grains with simulation time in the three systems. It is shown that the systems reach a steady state where the parabolic growth law is obeyed after about 2000 time steps and the number of grains is reduced to about one-third of the initial number after the same time duration. Some deviations from the parabolic growth law are observed in figure 6(*a*), especially at longer times. The main reason for the deviation is the existence of grid points not identified to belong to any grain (it should be reminded that the initial polycrystalline sample is prepared by distributing spherical grains). At the longer times, the number of grains is too small (slightly over 100), which can produce a large statistical fluctuation in the average grain size. On the other hand, the number of grains in figure 6(*b*) is statistically stable, because this quantity is free from the above-mentioned
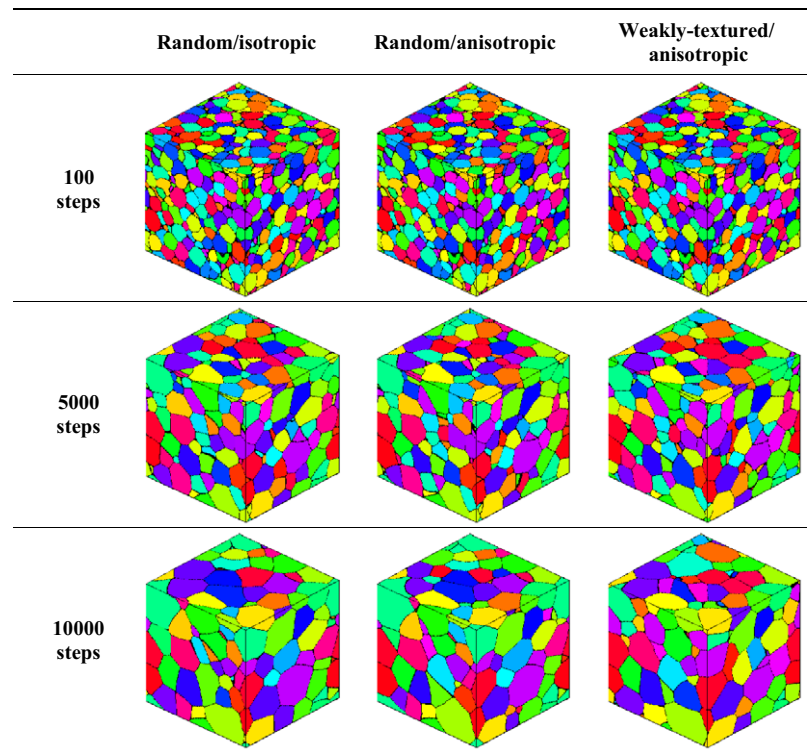
Figure 5. Microstructural evolution during the phase-field grain growth simulation in systems with a random crystallographic orientation and isotropic GB energy, with a random crystallographic orientation and anisotropic GB energy, and with a weak texture (relatively high portion of LAGBs) and anisotropic GB energy.

problem. Therefore, the results in figure 6(*b*) are used for further analyses of the effect of anisotropic GB energy.

What should be noted in figure 6(*b*) is that the number of remaining grains of the anisotropic system is slightly larger than in the isotropic system, especially when the initial portion of the LAGB (or low-energy GB) is larger. A larger number of remaining grains means that the grain growth kinetics are slower. The change in the portion of the LAGBs with simulation time is presented in table 1 for the three systems. The portion of the LAGBs is initially 1.4% in the samples with random crystallographic orientation, while that in the sample with a weak texture is initially 5.1%. The portion of the LAGBs remains unchanged when the GB energy is isotropic. However, when the GB energy is anisotropic, the portion increases from 1.5% to 2.2% in the sample with the random crystallographic orientation and from 5.1% to 10.1% in the sample with the weak texture. Grain growth is a procedure where relatively large grains grow further and relatively small grains shrink and disappear. The retardation of grain growth in the system with a large portion of low-energy GBs indicates that the existence of low-energy GBs has an effect on the overall grain growth kinetics in any form. It should be mentioned here that a slight retardation in grain growth kinetics due to anisotropic GB energy and mobility was also reported in a 2D phase-field simulation [29]. To understand the role of low-energy GBs in the grain growth procedure, further analyses are performed for the grain size and misorientation distribution.
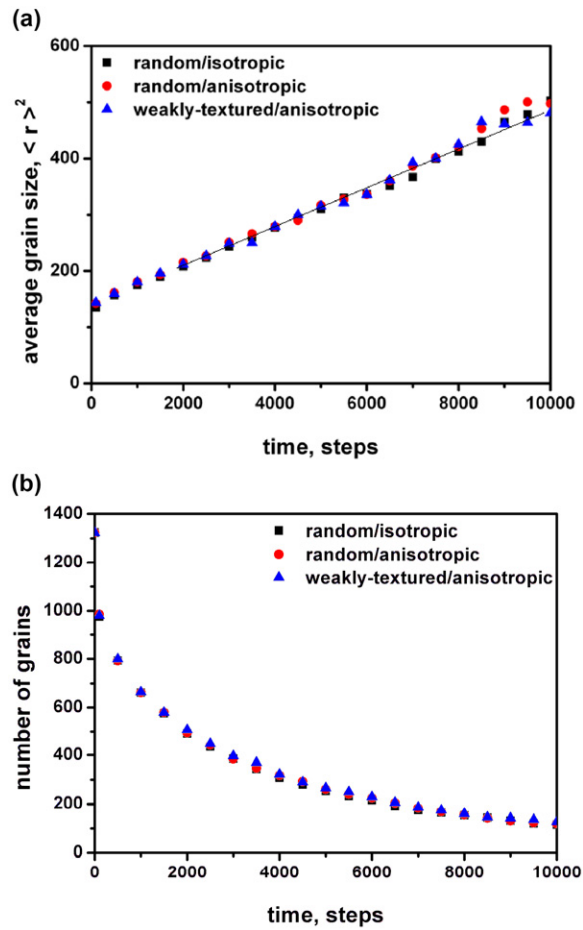
Figure 6. Time evolution of (*a*) the average grain size and (*b*) the number of remaining grains during the phase-field grain growth simulation.

Table 1. Change in the portion of LAGBs with simulation time for the systems with a random crystallographic orientation and isotropic GB energy, with a random crystallographic orientation and anisotropic GB energy, and with a weak texture (relatively high portion of LAGBs) and anisotropic GB energy.

	Random/ isotropic	Random/ anisotropic	Weakly textured/ anisotropic
100 steps	1.4%	1.5%	5.1%
10 000 steps	1.4%	2.2%	10.1%

In the case of normal grain growth, a rough log-normal distribution for data points in steel is already available from experiments [14, 43–45] for grain size distribution. The simulated grain size distribution (averaged in the range of 2000–10 000 steps) for the isotropic and the two anisotropic systems is compared with the log-normal distribution in figure 7. It is shown that the initial grain size distribution, which is far from the log-normal distribution,
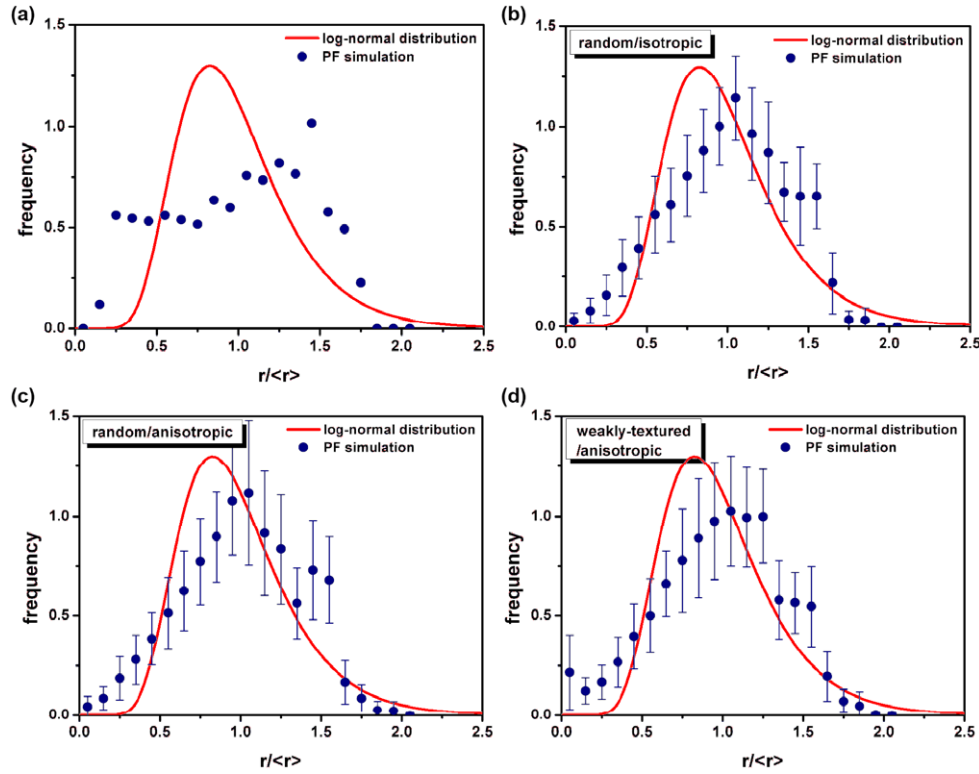
Figure 7. Grain size distributions in polycrystalline samples (*a*) in the initial state (100 steps) and (*b*), (*c*), (*d*) after phase-field grain growth simulations under different conditions, in comparison with a log-normal distribution for data points in steel [14, 43–45]. Here, the average (circle) and standard deviation (error bar) are taken from data points in a range of 2000 ∼ 10 000 steps.

changes toward the theoretical distribution in all three samples. The agreement between the log-normal distribution based on experimental data for steel and the present simulation is not good, probably because the effect of impurity atoms in experiments is not considered in the simulation; furthermore, the simulation sample is not large and the simulation time is not long enough to obtain a statistically stable equilibrium distribution. In particular, the significant deviation in the $r/\langle r \rangle = 1.0$–1.5 region is thought to originate from the initial distribution. One noticeable difference among the samples is that an exceptional peak is observed in the small grain size region of the sample with a weak initial texture (figure 7(*d*)). It is believed that the peak in the small grain size region originates due to the fact that small grains surrounded by low-energy GBs may survive longer than those surrounded by ordinary high-energy GBs.

The microstructural property considered next is the disorientation distribution among neighboring grains. A theoretical approach, the Mackenzie distribution [46, 47], is also available for cubic crystalline materials with a random texture. The disorientation distribution for the random/isotropic, random/anisotropic and weakly textured/anisotropic system at the beginning of the grain growth simulation and after the simulation is presented in figure 8, in comparison with the Mackenzie distribution. In samples with random crystallographic orientation, the initial misorientation distribution is already in good agreement with the
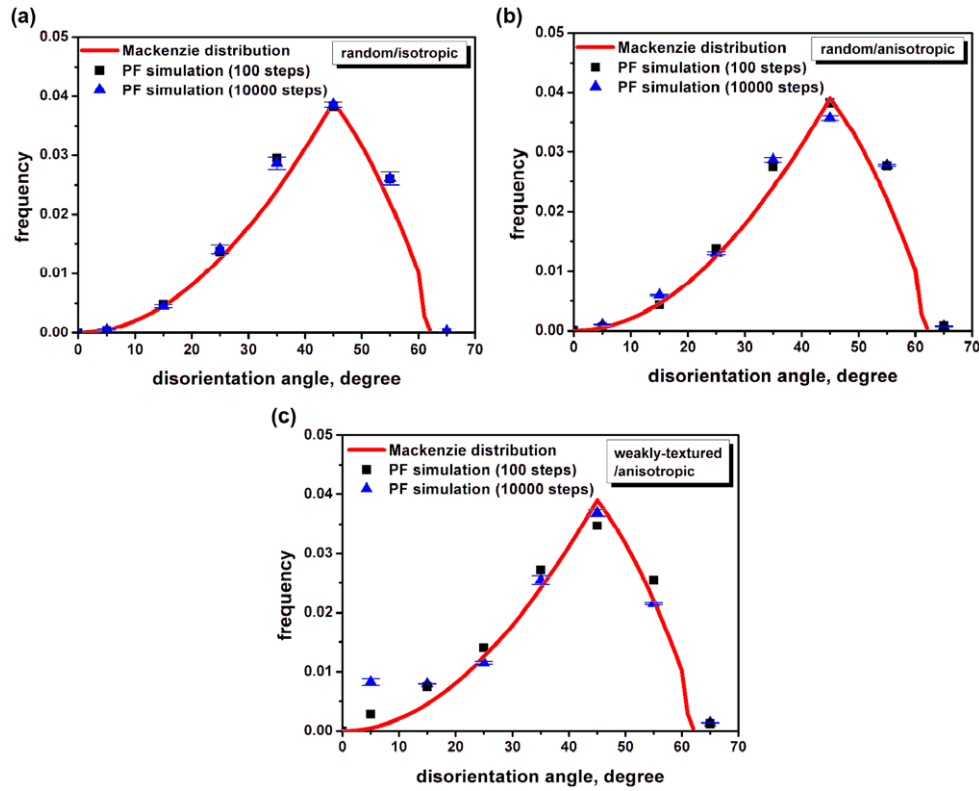
Figure 8. Disorientation distribution in polycrystalline samples before (100 steps) and after (10 000 steps) phase-field grain growth simulations under different conditions, in comparison with the Mackenzie distribution [46, 47]. The error bar in the misorientation distribution after 10 000 steps is the standard deviation in a range of 9500–10 500 steps.

Mackenzie distribution, which is to be expected. The disorientation distribution in those samples remains almost unchanged during the present simulation. On the other hand, the initial disorientation distribution with the weak texture shows a small positive deviation from the Mackenzie distribution, and the deviation increases as the grain growth proceeds, as can be seen in figure 8(*c*). This can be easily explained from the results presented in table 1, which show that the portion of low-angle or low-energy GBs in the weakly textured sample is initially larger than in samples with random crystallographic orientation, and the portion increases with simulation time.

It has been shown that the introduction of anisotropy in the GB energy changes the grain size and the misorientation distribution as well as the overall grain growth kinetics. The changes are rather meager when the polycrystalline sample has a random crystallographic orientation, but become clearer when the sample involves a non-random (relatively larger) portion of low-energy GBs. Even though no apparent effect of the anisotropic GB energy is observed on the overall microstructure shown in figure 5, it is expected that the existence of low-energy GBs would affect the local morphological evolution of relevant grains. To investigate this local behavior in more detail, a sample with a specially designed misorientation relationship is prepared for a grain growth simulation. Figure 9 shows such a sample with a $72 \times 72 \times 72$ grid system (about 30 grains). Here, the number ② grain has a Σ3 (or near Σ3) misorientation
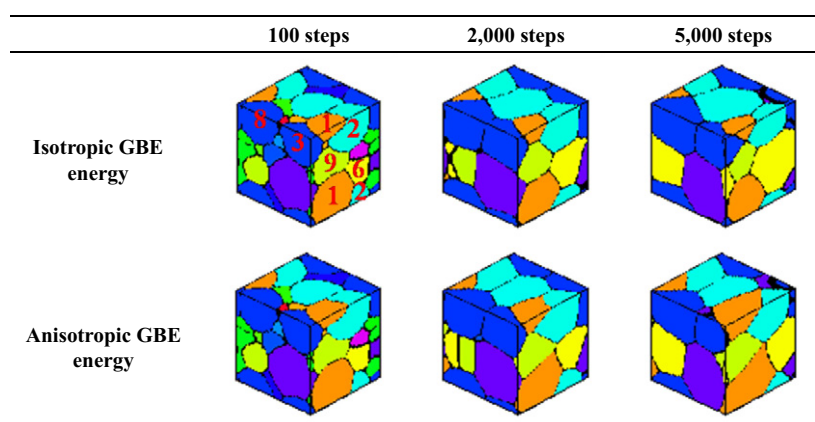
Figure 9. Local microstructural evolution during phase-field grain growth simulations based on isotropic GB energy and intentionally assigned anisotropic GB energy.

relationship with both the number ① grain and the number ⑨ grain. As a result, the number ① grain and number ⑨ grain share an LAGB. The $\Sigma3$ GB and the low-angle boundary have a lower energy than the other high-angle GBs in the sample. A phase-field simulation of grain growth is performed over this sample with the specially designed anisotropic GB energy. Another simulation is performed using the same sample, but with isotropic GB energy for comparison. The morphological evolution among those grains is clearly different depending on the condition (anisotropy) assigned to the GB energy, as shown in figure 9. It is shown that the microstructure evolves such that low-energy GBs (among grain numbers ①, ② and ⑨) increase their area. As a result, the number ① grain that shrinks with time under the isotropic GB energy condition does not show such behavior at all in the simulation with anisotropic GB energy. From the simulation results shown in figure 9, it can be confirmed that the anisotropic GB energy clearly affects the morphological evolution.

It has been shown that the anisotropy in the GB energy has an effect on both kinetics and morphological evolution during grain growth. The implementation of the GB energy database in phase-field modeling proposed in the present work enables a more realistic simulation of grain growth. In the present work, only the normal grain growth stage is covered due to the limitation in sample size and simulation time. However, the present multi-scale simulation technique (combining GB properties from an atomistic approach and mesoscale phase-field simulation) can be easily extended to the investigation of abnormal grain growth, which is of practical and technical importance [48–50]. Before more practical applications, many issues need to be addressed. First of all, the present GB energy values are those calculated at 0 K. The temperature dependence of the GB energy, i.e. the GB entropy term, needs to be introduced in the future. More importantly, the present GB energy database is for pure Fe. Alloying effects, especially the effect of GB segregation of alloying elements on the GB energy, need to be introduced for a more realistic simulation of phase transformations in practical alloys. GB mobility may also be an important factor for realistic grain growth simulations, because the anisotropy in mobility is much larger than that in GB energy and can have dramatic effects on the grain growth kinetics [51, 52]. It should be mentioned here that the orientation dependence of the mobility (GB mobility database) can be easily included in the phase-field simulation using the framework proposed in the present work. Even with such additional work, it is believed that the present implementation of the GB energy database in phase-field modeling

can be the starting point for an advanced level of phase-field simulation. The phase-field grain growth simulation code that utilises the GB energy database for pure bcc Fe and is used in the present study is provided together with the database, as the online supplementary material to this article (stacks.iop.org/MSMSE/22/034004/mmedia).

5. Conclusion

A multi-scale 3D simulation technique for the microstructural evolution of polycrystalline materials is now available by combining phase-field modeling with a GB energy database obtained from an atomistic approach. The present phase-field simulations performed for grain growth in polycrystalline pure bcc Fe show that the introduction of anisotropy in the GB energy results in slower kinetics and a different morphological evolution, and the effect is amplified as the portion of low-angle, low-energy GBs increases. The present phase-field model can be easily extended for more realistic simulations of bcc/fcc phase transformations in steel and even for other material systems once suitable GB or interfacial energy databases are provided.

Acknowledgment

References

[1] Kim S G, Kim D I, Kim W T and Park Y B 2006 Computer simulations of two-dimensional and three-dimensional ideal grain growth *Phys. Rev.* E **74** 061605

[2] Steinbach I and Pezzolla F 1999 A generalized field method for multiphase transformations using interface fields *Physica* D **134** 385–93

[3] McKenna I M, Gururajan M P and Voorhees P W 2009 Phase field modeling of grain growth: effect of boundary thickness, triple junctions, misorientation, and anisotropy *J. Mater. Sci.* **44** 2206–17

[4] Burke J E and Turnbull D 1952 *Progress in Metal Physics* vol 3 (London: Pergamon) pp 220–92

[5] Thompson C V 2000 *Grain Growth and Evolution of Other Cellular Structures Solid State Physics* vol 55 (San Diego, CA: Academic) pp 270–314

[6] Warren J A and Boettinger W J 1995 Prediction of dendritic growth and microsegregation patterns in a binary allot using the phase-field method *Acta Metall. Mater.* **43** 689–703

[7] Karma A and Rappel W J 1998 Quantitative phase-field modeling of dendritic growth in two and three dimensions *Phys. Rev.* E **57** 4323–49

[8] Tiaden I, Nestler B, Dipers H J and Steinbach I 1998 The multiphase-field model with an integrated concept for modelling solute diffusion *Physica* D **115** 73–86

[9] Kim S G, Kim W T and Suzuki T 1999 Phase-field model for binary alloys *Phys. Rev.* E **60** 7186–97

[10] Singer-Loginova I and Singer H M 2008 The phase field technique for modeling multiphase materials *Rep. Prog. Phys.* **71** 106501

[11] Steinbach I 2009 Phase-field models in materials science *Modelling Simul. Mater. Sci. Eng.* **17** 073001

[12] Chen L Q and Yang W 1994 Computer simulation of the domain of a quenched system with a large number of nonconserved order parameters: the grain-growth kinetics *Phys. Rev.* B **50** 15752

[13] Fan D and Chen L Q 1997 Computer simulation of grain growth using a continuum field model *Acta Mater.* **45** 611–22

[14] Krill C E III and Chen L Q 2002 Computer simulation of 3-D grain growth using a phase-field model *Acta Mater.* **50** 3057–73

[15] Steinbach I, Pezzolla F, Nestler B, Seeßelberg M, Prieler R, Schmitz G J and Rezende J L L 1996 A phase field concept for multiphase systems *Physica* D **94** 135–47

[16] Kamachali R D and Steinbach I 2012 3-D phase-field simulation of grain growth: topological analysis versus mean-field approximations *Acta Mater.* **60** 2719–28

[17] Nestler B, Wheeler A A and Garcke H 2003 Modelling of microstructure formation and interface dynamics *Comput. Mater. Sci.* **26** 111–9

[18] Kazaryan A, Wang Y, Dregia S A and Patton B R 2001 Grain growth in systems with anisotropic boundary mobility: analytical model and computer simulation *Phys. Rev.* B **63** 184102

[19] Kazaryan A, Wang Y, Dregia S A and Patton B R 2002 Grain growth in anisotropic systems: comparison of effects of energy and mobility *Acta Mater.* **50** 2491–502

[20] Kazaryan A, Patton B R, Dregia S A and Wang Y 2002 On the theory of grain growth in systems with anisotropic boundary mobility *Acta Mater.* **50** 499–510

[21] Suwa Y, Saito Y and Onodera H 2007 Three-dimensional phase field simulation of the effect of anisotropy in grain-boundary mobility on growth kinetics and morphology of grain structure *Comput. Mater. Sci.* **40** 40–50

[22] Suwa Y and Saito Y 2005 Phase field simulation of the effect of anisotropy in grain boundary energy on growth kinetics and morphology of grain structure *Mater. Trans.* **46** 1208–13

[23] Kobayashi R, Warren J A and Carter W C 2000 A continuum model of grain boundaries *Physica* D **140** 141–50

[24] Pusztai T, Bortel G and Granasy L 2005 Phase field theory of polycrystalline solidification in three dimensions *Europhys. Lett.* **71** 131–7

[25] Pusztai T, Tegze G, Toth G I, Környei L, Bansel G, Fan Z and Granasy L 2008 Phase-field approach to polycrystalline solidification including heterogeneous and homogeneous nucleation *J. Phys.: Condens. Matter* **20** 404205–21

[26] Kim S G, Kim W T, Suzuki T and Ode M 2004 Phase-field modeling of eutectic solidification *J. Cryst. Growth* **261** 135–58

[27] Moelans N, Blanpain B and Wollants P 2008 Quantitative analysis of grain boundary properties in a generalized phase field model for grain growth in anisotropic systems *Phys. Rev.* B **78** 024113

[28] Moelans N, Blanpain B and Wollants P 2008 Quantitative phase-field approach for simulating grain growth in anisotropic systems with arbitrary inclination and misorientation dependence *Phys. Rev. Lett.* **101** 025502

[29] Upmanyu M, Hassold G N, Kazaryan A, Holm E A, Wang Y, Patton B and Srolovitz D J 2002 Boundary mobility and energy anisotropy effects on microstructural evolution during grain growth *Interface Sci.* **10** 201

[30] Shimizu R and Harase J 1989 Coincidence grain boundary and texture evolution in Fe–3%Si *Acta Metall.* **37** 1241–9

[31] Rajmohan N, Szpunar J A and Hayakawa Y 1999 Importance of fractions of highly mobile boundaries in abnormal growth of Goss grains *Mater. Sci. Eng.* A **259** 8–16

[32] Kim H K, Ko W S, Lee H J, Kim S G and Lee B J 2011 An identification scheme of grain boundaries and construction of a grain boundary energy database *Scr. Mater.* **64** 1152–5

[33] Olmsted D L 2009 A new class of metrics for the macroscopic crystallographic space of grain boundaries *Acta Mater.* **57** 2793

[34] Grimmer H 1974 Disorientations and coincidence rotations for cubic lattices *Acta Crystallogr.* A **30** 685–8

[35] Kim S G and Park Y B 2008 Grain boundary segregation, solute drag and abnormal grain growth *Acta Mater.* **56** 3739–53

[36] Kim S G 2010 Prediction of secondary recrystallization texture by using anisotropy database of grain boundary energy and mobility *Report on the POSCO-Project* unpublished

[37] Cahn J W and Hoffman D W 1974 A vector thermodynamics for anisotropic surfaces: II. Curved and faceted surfaces *Acta Metall.* **22** 1205–14

[38] Voorhees P W, Coriell S R, McFadden G B and Sekerka R F 1984 The effect of anisotropic crystal–melt surface tension on grain boundary groove morphology *J. Cryst. Growth* **67** 425–40

[39] Gruber J, Ma N, Wang Y, Rollett A D and Rohrer G S 2006 Sparse data structure and algorithm for the phase field method *Modelling Simul. Mater. Sci. Eng.* **14** 1189–95

[40] Vedantam S and Patnaik B S V 2006 Efficient numerical algorithm for multiphase field simulations *Phys. Rev.* E **73** 016703

[41] Wits J J, Kop T A, van Leeuwen Y, Seitsma J and van der Zwaag S 2000 A study on the austenite-to-ferrite phase transformation in binary substitutional iron alloys *Mater. Sci. Eng.* A **283** 234–41

[42] Atkinson H V 1988 Theories of normal grain growth in pure single phase systems *Acta Metall.* **36** 469–91

[43] Okazaki K and Conrad H 1972 Grain size distribution in recrystallized alpha-titanium *Mater. Trans. JIM* **13** 198–204

[44] Rhines F N and Patterson B R 1982 Effect of the degree of prior cold work on the grain volume distribution and the rate of grain growth of recrystallized aluminum *Metall. Trans.* A **13** 985–93

[45] Pande C S 1987 On a stochastic theory of grain growth *Acta Metall.* **35** 2671–8

[46] Mackenzie J K 1964 The distribution of rotation axes in a random aggregate of cubic crystal *Acta Metall.* **12** 223–5

[47] Mackenzie J K 1958 Second paper on statistics associated with the random disorientation of cubes *Biometrika* **45** 229–40

[48] Hwang N M 1998 Simulation of the effect of anisotropic grain boundary mobility and energy on abnormal grain growth *J. Mater. Sci.* **33** 5625

[49] Rollett A D, Srolovitz D J and Anderson M P 1989 Simulation and theory of abnormal grain growth–anisotropic grain boundary energies and mobilities *Acta Metall.* **37** 1227

[50] Srolovitz D J, Grest G S and Anderson M P 1985 Computer simulation of grain growth: V. Abnormal grain growth *Acta Metall.* **33** 2233

[51] Gottstein G and Shvindlerman L S 1999 *Grain Boundary Migration in Metals : Thermodynamics, Kinetics, Applications* (Boca Raton, FL: CRC Press)

[52] Holm E A and Foiles S M 2010 How grain growth stops: a mechanism for grain-growth stagnation in pure materials *Science* **328** 1138